Appl Nanosci
DOI 10.1007/s13204-017-0615-6

ORIGINAL ARTICLE

Eco-friendly biosynthesis, anticancer drug loading and cytotoxic effect of capped Ag-nanoparticles against breast cancer

M. Naz[1] · N. Nasiri[2,4] · M. Ikram[3] · M. Nafees[3] · M. Z. Qureshi[1] · S. Ali[3] · A. Tricoli[2]

Received: 14 August 2017 / Accepted: 4 October 2017

Abstract The work aimed to prepare silver nanoparticles (Ag-NPs) from silver nitrate and various concentrations of the seed extract (*Setaria verticillata*) by a green synthetic route. The chemical and physical properties of the resulting Ag-NPs were investigated by X-ray diffraction (XRD), transmission electron microscopy (TEM), Fourier transform infrared (FTIR) spectrometry and ultraviolet–visible (UV–Vis) spectrophotometry. Anticancer activity of Ag-NPs (5–20 nm) had dose-dependent cytotoxic effect against breast cancer (MCF7-FLV) cells. The in vitro toxicity was studied on adult earthworms (Lumbricina) resulting in statistically significant ($P < 0.05$) inhibition. The prepared NPs were loaded with hydrophilic anticancer drugs (ACD), doxorubicin (DOX) and daunorubicin (DNR), for developing a novel drug delivery carrier having significant adsorption capacity and efficiency to remove the side effects of the medicines effective for leukemia chemotherapy.

✉ M. Ikram
dr.muhammadikram@gcu.edu.pk

✉ M. Nafees
rajvi_gcu@yahoo.com

1 Biochemistry Lab, Department of Chemistry, Government College University Lahore, Lahore 54000, Pakistan

2 Nanotechnology Research Laboratory, Research School of Engineering, Australian National University, Canberra 2601, Australia

3 Solar Cell Applications Research Lab, Department of Physics, Government College University Lahore, Lahore 54000, Pakistan

4 Institute for Biomedical Materials and Devices, Faculty of Science, University of Technology Sydney, Sydney 2007, Australia

Published online: 23 October 2017

Keywords Drug loading · Seed extract · Cytotoxicity · Anthelmintic activity · Ag-NPs

Introduction

Nobel metal nanoparticles (NPs) such as silver (Ag), gold (Au) and platinum (Pt) have attracted significant attention due to their potential medicinal properties for use as sensor and for biomedical imaging (Zhang et al. 2017; Zhang et al. 2016). Among these, Ag-NPs have unique optical, electrical and biomedical properties, making them suitable for biosensing, imaging and catalysis, as medicine and in nano device fabrication and drug delivery (Ismail et al. 2017; Lee and El-Sayed 2006; Nair and Laurencin 2007; Upendra et al. 2015). There is a growing demand to develop eco-friendly methods, which are free from toxic substances, for the synthesis of NP (Lade and Patil 2017; Smetana et al. 2005; Yu 2007; Zhang et al. 2009). Various techniques have been used to prepare Ag-NPs such as thermal decomposition, chemical reduction, microwave-assisted synthesis, biological reduction and laser-mediated synthesis (Navaladian et al. 2007; Krishna et al. 2016; Tolaymat et al. 2010; Zamiri et al. 2011). Among these, biosynthesis employs significantly lower quantities of toxic chemicals and thus provides an attractive alternative for the synthesis of environmentally benign nanoparticles.

Various research groups have explored the role of seed extracts from different plants such as *Linum usitatissimum* L., *Artocarpus heterophyllus lam.*, *Cola nitida,* pomegranate, *Elettaria cardamomum, Melia azedarach* and *Medicago sativa* (Azeez et al. 2017; Lukman et al. 2011; Kokina et al. 2013; Khan et al. 2011; Jagtap and Bapat 2013) for the biosynthesis of environment-friendly Ag-NPs. Recently, a green eco-friendly route was employed

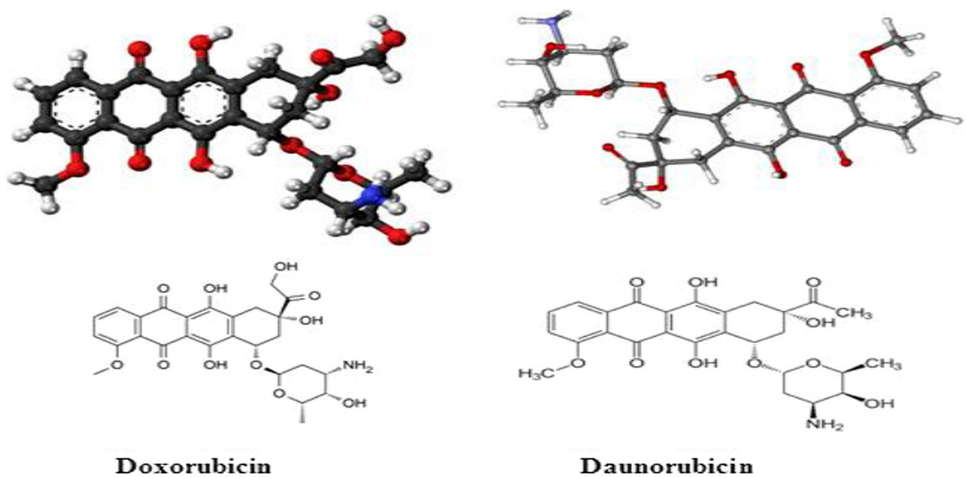

Fig. 1 Molecular structure of DOX and DNR

for the synthesis of stable NPs using the extracts derived from *Setaria verticillata* seeds. *Setaria verticillata* is a grassy annual plant that belongs to the family of Poaceae. Historically, it has found different purposes in different regions such as preparing malt for beer in South Africa, making porridge in Nambia and as nutritious and palatable forage for livestock (Holm et al. 1977).

Since the last decade, nanoparticles-based drug loading has gained the attraction of researchers due to its potential to reduce the expected side effect produced by conventional methods. UV–visible spectroscopy is the most convenient, economical, accurate and extensively used method to estimate drug loading. In this study, Ag-NPs with various concentrations of the seed extract (*Setaria verticillata*) were prepared by a green synthetic route. The cytotoxicity was evaluated against MCF7-FLV breast cancer cells, and in vitro anthelmintic screening of NPs was performed on adult earthworms as model due to their physiological and anatomical resemblance to human intestinal parasites. In addition, NPs were used for anticancer drug (ACD), DOX and DNR, loading. Here, a variety of techniques, including XRD, TEM, FTIR spectrometry and UV–Vis spectroscopy were used to characterize the biosynthesized Ag-NPs as a function of the concentration of *Setaria verticillata* seed extract.

Materials and methods

Materials

Silver nitrate was obtained from Sigma-Aldrich. The MCF7-FLV1000 cell was provided by the Department of Cancer Biology and Therapeutics, John Curtin School of Medicine, Australian National University (ANU). Anticancer drugs doxorubicin hydrochloride [DOX, Pharmedic Laboratories (Pvt.) Ltd] and daunorubicin [DNR, Pharmedic Laboratories (Pvt.) Ltd] were used for drug loading. *Setaria verticillata* seeds were collected from the Mozang region in Lahore, Pakistan, and identified at the Department of Botany Government College University (GCU) Lahore, Voucher No. GC.Herb.Bot.2914. Adult earthworms (Lumbricina) were collected locally from River Ravi region Lahore. The identification of Lumbricina was done according to standard methods (Sims and Gerard 1985). The earthworm's body was cylindrical in shape and the posterior end was flattened dorsoventrally. The body length of the adult earthworm ranged between 100 and 300 mm and the diameter varied between 2 and 6 mm. External transverse furrows dividing the body into a series of similar linear compartments were also present on the earthworm's body. Figure 1 represents the structure of anticancer drugs used in the experiment (Doxorubicin 2017; Daunorubicin 2017).

Preparation of plant extract and synthesis of Ag-NPs

Setaria verticillata (SV) seeds were cleaned using distilled water three times prior to use. 10 g of seeds was dipped in 100 ml of double distilled water for 24 h (h). The aqueous SV extract was filtered and then kept in the refrigerator for further experiments (Sharma and Jeevanandam 2013). For the preparation of Ag-NPs, different concentrations of SV extract, namely 10 vol% (10 SV), 20 vol% (20 SV), 30 vol% (30 SV) and 40 vol% (40 SV), were mixed with 1 mM aqueous $AgNO_3$ solution, in which $AgNO_3$ was reduced by the SV extract. The reduction of Ag^+ was confirmed by a distinct change of color as shown in Fig. 2a.

Particle characterization

UV–visible spectrophotometer (TECAN infinite M200PRO) was used to monitor the absorption spectra of various concentrations of Ag-NPs. The mean crystal size, phase composition and other structural information of Ag-

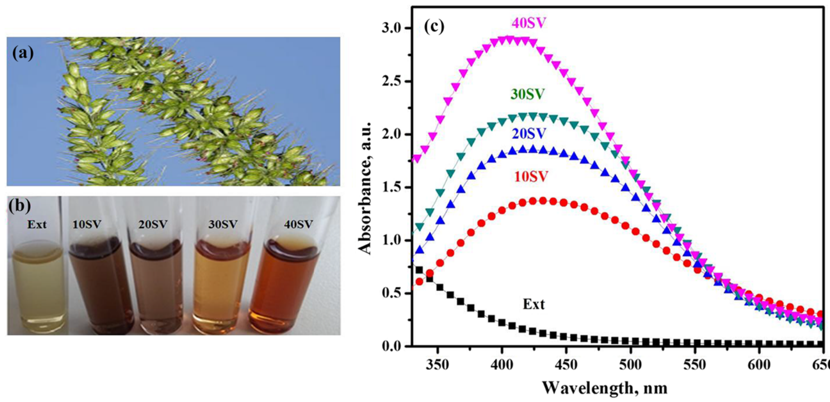

Fig. 2 **a** *Setaria verticillata* seeds. **b** Visual appearance of vials containing seed extract and different concentrations of SV seed extract, from 10 up to 40 vol% (left to right), mixed with 1 mM silver nitrate. **c** UV–visible absorption spectra for seed extract and different concentrations of extract from 10 vol% (10 SV) up to 40 vol% (40 SV) in making Ag-NPs

NPs were obtained by XRD using Bruker system (XRD, D2 Phaser, USA) equipped with Cu Kα radiation of average wavelength 1.54059 Å. The size distribution of Ag-NPs was characterized by TEM using Hitachi H7100FA TEM at 100 kV. Energy-dispersive X-ray spectroscopy (EDX) analysis was also conducted using Hitachi H7100FA TEM. The functional groups in the resultant samples were investigated using BRUKER ALPHA Platinum ATR spectrometer.

Neutral red assay

MCF7-FLV1000 cells were routinely seeded in media (RPMI) supplemented with 10% fetal bovine serum (FBS), 10 mM HEPES and 2 g/L $NaHCO_3$ at 37 °C with 5% CO_2, with every fourth passage supplemented with 0.5 nM flavopiridol to maintain drug resistance/selection pressure. Cells were grown in 96-well plates at $\sim$ 50% confluence and incubated overnight to establish a monolayer. Cells were treated with 40SV nanoparticles diluted in media for 48 h (quadruplicate wells per treatment). After treatment, cells were incubated for 3 h in neutral red (33 µg mL^{-1}) medium, washed twice with PBS and lysed with 75% methanol:25% acetic acid solution. A microplate reader was used to measure the absorbance at 540 nm. The viability of the treated cells was represented as the percentage of the untreated control. The activity of the 40SV nanoparticles was compared to free Ag present in $AgNO_3$ and to equivalent amounts of unprocessed plant extract.

Drug loading

Firstly, 5 mg of DOX and DNR was dissolved in 100 mL water and stirred to prepare individual drug solutions. These solutions were examined between 400 and 600 nm by UV–visible spectrophotometer for use as control sample (0 min). After that, 10 mg Ag-NPs was added to each solution with particle concentration 100 mg L^{-1} and kept in an orbital shaker at moderate frequency. The adsorption and concentration behaviors of DOX and DNR were recorded by taking 2.5 mL of unbound drug supernatant at various time intervals (30, 60, 120, 240 and 480 min.) for measuring the drug loading capacity evaluated by UV–visible absorption at 480 nm.

Loading efficiency

The loading capacity (LC) and loading efficiency (LE) of drugs (DOX, DNR) were calculated by Eqs. (1) (Mashhadizadeh and Diva 2012) and (2) (Mashhadizadeh and Diva 2012; Sabeti et al. 2014), respectively.

$$\text{LC of drug}\left(\frac{\text{mg}}{\text{mg}}\right) = \frac{(\text{Drug}_\text{i})-(\text{Drug}_\text{f})}{(\text{Drug}_\text{c})}, \qquad (1)$$

$$\%\ \text{LE of drug} = \frac{(\text{Drug}_\text{i})-(\text{Drug}_\text{f})}{(\text{Drug}_\text{i})} \times 100. \qquad (2)$$

(Drug_i) is the initial amount (mg) of the drug, (Drug_f) the free drug that remains in the supernatant and (Drug_c) the amount (mg) of carrier (Ag-NPs drug cargo).

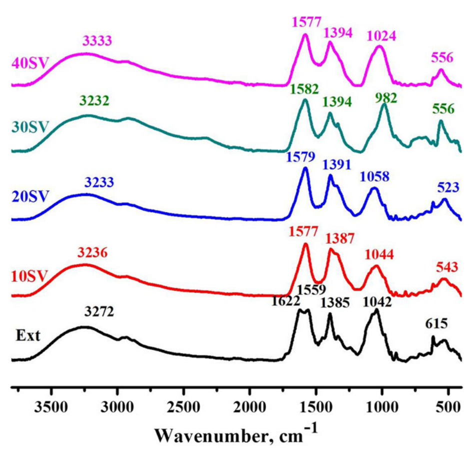

Fig. 3 FTIR spectra of extract and biosynthesized silver nanoparticles with different extract concentrations from 10 vol% (10 SV) up to 40 vol% (40 SV)

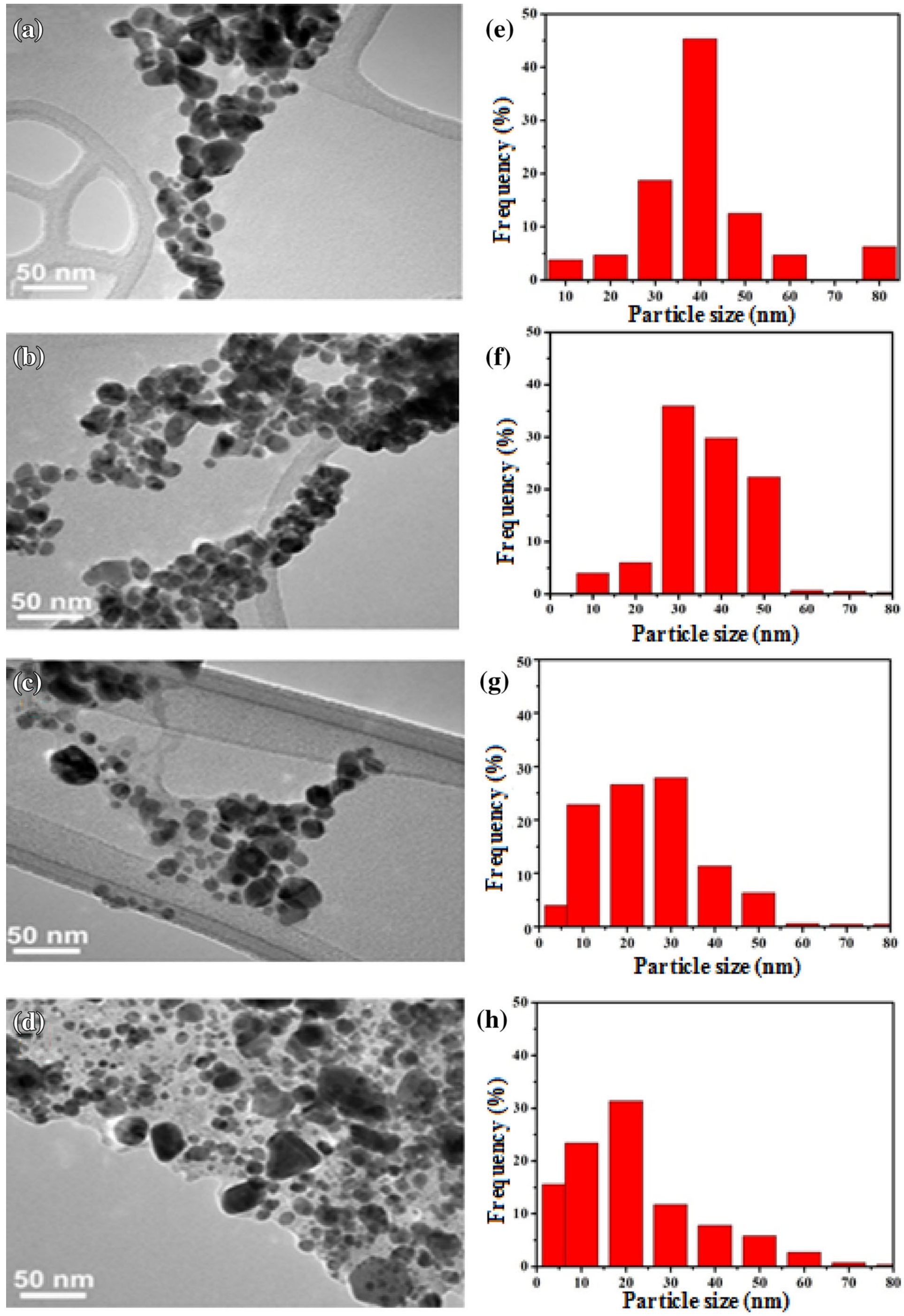

Fig. 4 TEM images of biosynthesized silver nanoparticles (**a**–**d**) and their corresponding size distribution (**e**–**h**) using SV seed extract at different concentrations of **a, e** 10 SV; **b**, **f** 20 SV; **c**, **g** 30 SV and **d**, **h** 40 SV

Anthelmintic activity

In vitro anthelmintic study of Ag-NPs was evaluated in ten Petri dishes containing four adult earthworms each and preserved in phosphate-buffered solution (50 mL). NPs were used for in vitro trials and each dilution had 6 and 12 µg mL^{-1}separately, while the single dose of levamisole HCl 0.55 µg mL^{-1} acted as a positive control and no treatment was given to a Petri plate which acted as the negative control. The in vitro anthelmintic potential of NPs was determined on the basis of number of dead earthworms after 3 h of incubation at 37 °C, similar to previous research (Amin et al. 2009).

Results and discussion

Figure 2c shows the UV–visible spectra of Ag-NPs synthesized with different concentrations of the seed extract. It can be observed that a broad absorption peak appeared between 350 and 550 nm after $AgNO_3$ solution reacted with SV. Decreasing the SV concentration from 40 to 10 vol% shifted the absorption to longer wavelengths, accompanied by a significant decrease in the absorption intensity. This shift and decrease in absorption intensity are well reflected in the sharp change in sample color upon decreasing the SV concentration (Fig. 2a).

The FTIR spectra of the Ag-NPs synthesized at the various SV concentrations was obtained to identify the functional groups present (Fig. 3). This is critical as functional groups not only interact with metal salts, but also play an important role in the nanoparticle synthesis (Babu and Gunasekaran 2009; Bar et al. 2009). The absorbance peak located at 3272 cm^{-1} corresponds to amine N–H (Velmurugan, et al. 2011) and alcoholic O–H stretching vibrational modes. The peaks at 1622 and 1559 cm^{-1} suggest the presence of aromatic –C=C stretching vibrations, which are usually typical for the amide band of polypeptides. The absorption bands at 1385, 1042 and 615 cm^{-1} show the stretching vibration of the amide, alkene group and most probably the C–O group of polyols, (Ramamurthy et al. 2013) respectively. Notably, the peaks at 3272, 1559, 1385, 1042 and 615 cm^{-1} of the seed extract are shifted in the biosynthesized Ag-NPs. In particular, the peak at 3272 cm^{-1} of the SV seed exudate shifted to higher wavelength indicating surface binding to Ag-NPs, while the 1622 cm^{-1} peak shifted to lower wavelength (1577 cm^{-1}) indicating reduction of $AgNO_3$ to Ag-NPs (Ramar et al. 2015). Figure 4a–d shows the representative TEM images of four Ag-NPs batches synthesized with different seed extract concentrations. The size and shape of the particle are influenced by the seed extract concentration. The size of the NPs decreased with increase in the seed extract concentration. At 10 vol% of the extract, the formation of large NPs of 35 nm was observed. At 40 vol%, smaller NPs of 20 nm were formed. The average particle sizes (d_{TEM}) analyzed from count size distribution were 40, 38, 27 and 22 nm, respectively, for samples synthesized at 10–40 SV (Fig. 4). At the same time, the geometric standard variation also ranged from $\sim$ 40 nm at 10 vol% to $\sim$ 22 nm at 40 vol%.

EDX analysis was conducted to probe the composition of biosynthesized Ag-NPs. The three characteristic Ag peaks can be observed at approximately 3, 22 and 25 keV (Fig. 5). A spectrum at 3 keV is the typical energy value for metallic silver nano crystallites (Magudapathy et al. 2001). In addition, the spectral signatures of carbon and sulfur were also observed, indicating that extracellular biomoieties were adsorbed on the surface or in the vicinity of metal nanoparticles. The Cu and Al signals come from the grid and instrument, respectively.

Figure 6 shows the XRD pattern of the Ag-NP powders. A number of Bragg diffraction peaks, indexed as (111), (200), (220) and (311) with corresponding 2θ values of 38°,44°, 64° and 76° confirm the crystallinity and the face-centered cubic Ag structure (JCPDS 04-0783) (Priyadharshini et al. 2014). The average crystal size obtained from the Scherrer equation (d_{XRD}) was 13.7, 9, 10.9 and 10.3 nm from 10 to 40 SV, respectively.

Figure 7a, b represents the absorption spectra of hydrophilic anticancer drug (DOX and DNR) supernatants collected at various time intervals (0–480 min), and the highest peak intensity of drugs at zero time ($t = 0$) was for the control sample (free from Ag–NO_3). Absorbance of anticancer drugs decreases with the passage of time due to adsorption of drug on the surface of Ag-NP. The maximum amount of drug is adsorbed after 480 min. Figure 8a illustrates the relevant absorption of drugs. There is a rapid decrease in the first 30 min due to availability of large surface area, high adsorption capacity and fast adsorption

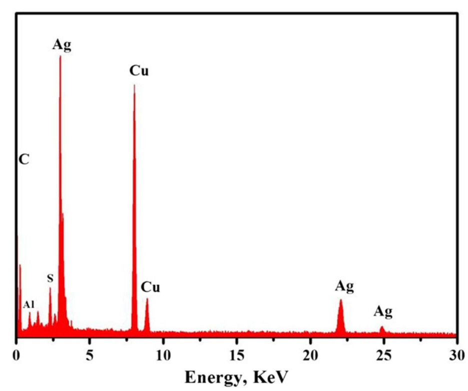

Fig. 5 EDX of Ag-NPs prepared with SV seed extract

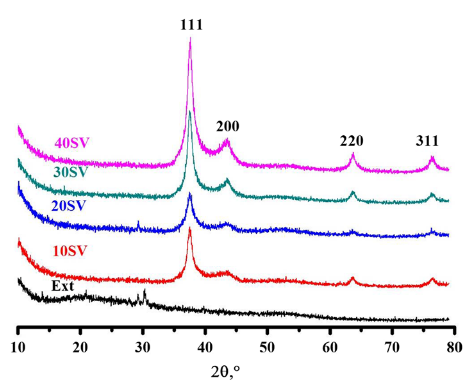

Fig. 6 XRD patterns of extract and biosynthesized Ag-NPs with different concentrations of seed extract from 10 vol% up to 40 vol% (40 SV)

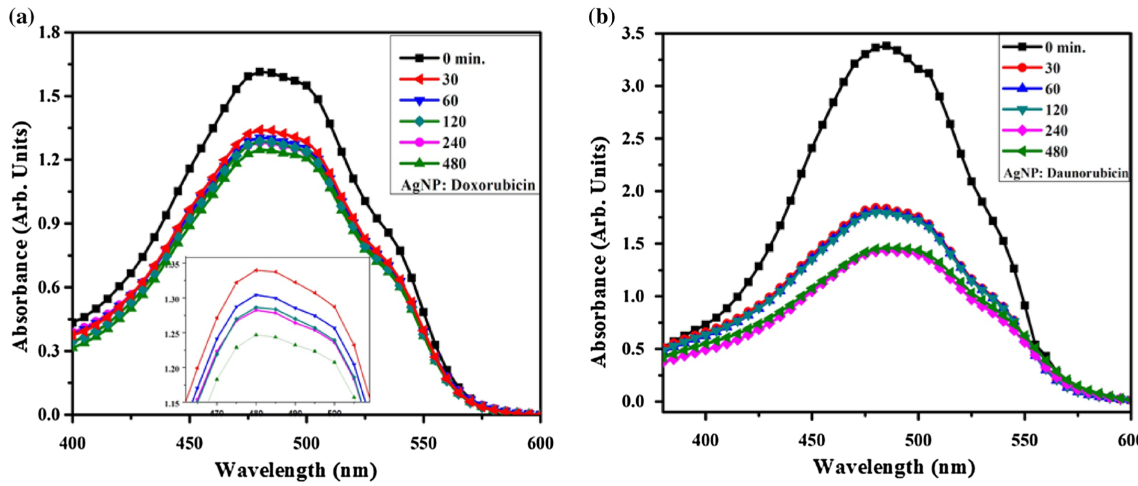

Fig. 7 Absorption spectra of **a** DOX and **b** DNR for various contact time ranges from 0 to 480 min

rate of ACD on Ag-NP. The possible mechanisms involved are as follows: (a) The electrostatic interaction of negatively charged bio-moieties on the surface of Ag-NP can easily attract the positively charged ACD molecules adsorbed onto the surface of NPs (Lin and Xing 2008a, b).

(b) There is hydrogen bonding due to a variety of oxygen-containing functional groups present in phytosynthesized Ag-NPs such as −C=O, −COOH and −OH. These functional groups make Ag-NPs more suitable for the adsorption of comparatively low molecular weight compounds (Lin and Xing 2008a, 2008b), because the hydrogen bonding between ACD and Ag-NP may occur in four ways: (1) –COOH of Ag-NPs and –OH of ACD; (2) –COOH of Ag-NPs and $-NH_2$ of ACD; (3) –OH of Ag-NPs and –OH of drugs; and (4) –OH of Ag-NPs and $-NH_2$ of ACD (Depan et al. 2011).

Figure 8b depicts the efficiency of DOX and DNR after 480 min. DOX showed relatively low absorption (45%) as compared to DNR (77.5%). However, DOX presented high loading efficiency and loading capacity of 55% (550 mg g^{-1}) and 27.5% (275 mg g^{-1}) relative to DNR, 22.5% (225 mg g^{-1}) and 11.25% (112.5 mg g^{-1}) (Teo et al. 2017).

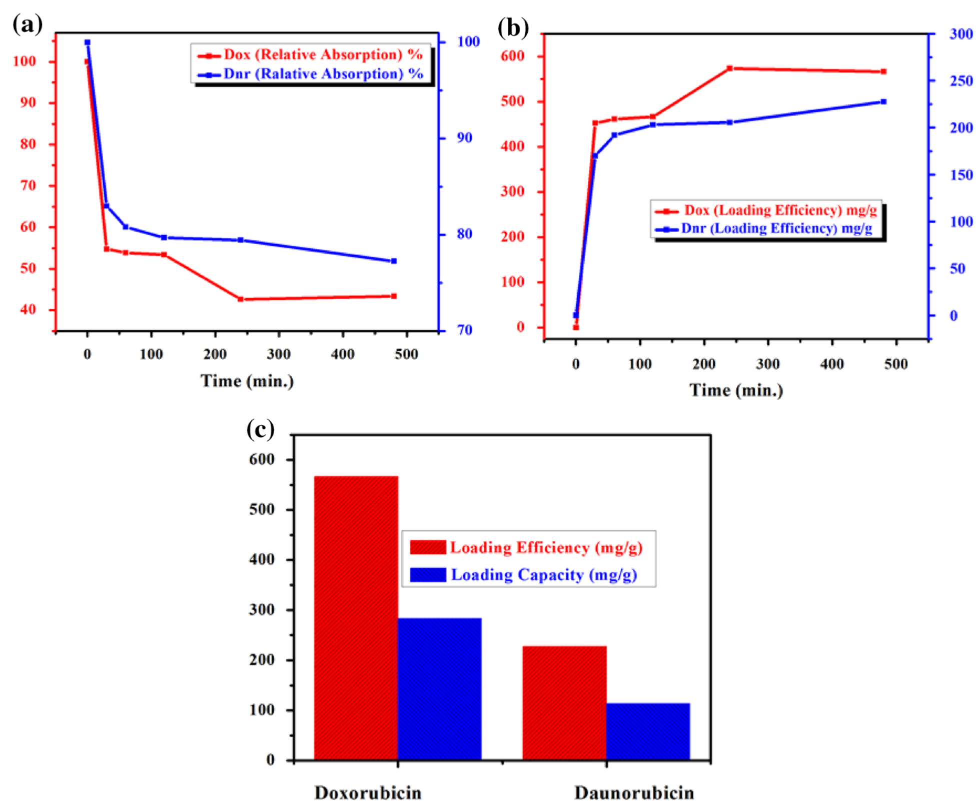

Fig. 8 **a** Relative absorption, **b** loading capacity and **c** comparison of LC and LE for DOX and DNR

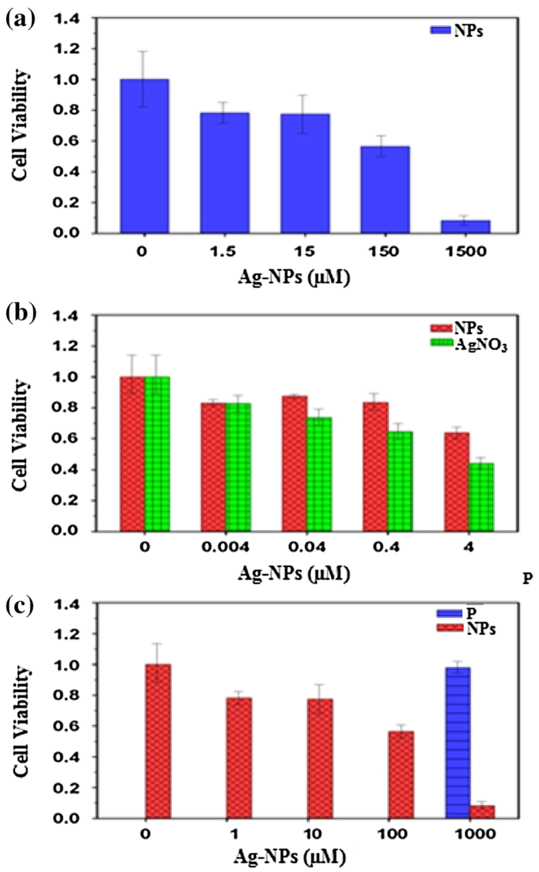

Fig. 9 Effect of Ag-NPs, $AgNO_3$ and plant extract on cell viability of MCF7-FLV breast cancer cells measured by neutral red uptake assay. **a** Cells were treated with Ag-NPs at various concentrations (0–1500 µM) of Ag-NPs. **b** Comparative analysis of equimolar concentrations of Ag present as either Ag-NPs or $AgNO_3$ against breast cancer cells. **c** Effect of equivalent amounts of plant extract present as Ag-NPs or plant extract on MCF7-FLV cells (0–1000 µM plant extract equivalents). The results are expressed as the mean ± SD of one experiment, representative of two separate experiments

The DOX- and DNR-loaded Ag-NPs showed efficient and remarkable loading efficiency (55, 22.5)% and capacity (27.5, 11.25)%, respectively

In the current study, the cytotoxicity of 40 SV-Ag-NPs was also evaluated on MCF7-FLV breast cancer cells in vitro by the neutral red method. The synthesized Ag-NPs of size 5–20 nm had a dose-dependent cytotoxic effect. Figure 9a–c represents three different experiments. Various concentrations of colloidal nanoparticle were treated against MCF7-FLV, showing IC_{50} at 136 µM Ag-NPs as in Fig. 9a (Satapathy et al. 2013). Figure 9b represents the comparative analysis of molar-equivalent Ag as either Ag-NPs- or $AgNO_3$-indicated toxicity in a concentration-dependent manner. Cell viability is reduced by 50% when treated with $AgNO_3$ and 35% with Ag-NPs at the concentration of 4 µM silver nanoparticles, indicating that unpackaged Ag is more cytotoxic than the nanoparticles. $NaNO_3$ at the same concentrations did not show any cytotoxicity (data not shown). The relative cytotoxic effect of Ag-NPs and equivalent amounts of plant extract on MCF7-FLV cells (0–1000 µM) was examined. The plant extract did not cause any significant growth inhibition in the cells, but SV-Ag-NPs had IC_{50} at 18 µg mL^{-1} and cell viability was reduced by 90% at 100 µg mL^{-1} Ag-NPs.

Ag-NPs synthesized with *Coleus amboinicus* extracts induced toxicity at 30 and 50 µg mL^{-1} respectively, to EAC cell lines indicating concentration-dependent cytotoxicity (Subramanian and Suja 2012). Ag-NPs (9–32 nm) had dose-dependent toxic effects on prostate cancer (PC-3) cells, ≈ 50% of cells died at 5–10 µg $mL^{-1}$and IC50 was > 10 µg mL^{-1}(Firdhouse and Lalitha 2013; He et al. 2016). The size and dose of Ag-NP involved in the test played important roles on their toxicity (Carlson 2008; Söderstjerna 2014). Small size nanoparticles of *Setaria verticillata*, *Potentilla fulgens, G. neo-japonicum* and

Table 1 Comparative analysis of plant-derived Ag-NPs on cancer cells

Plant-derived Ag-NPs	Cell line	IC50 µg mL^{-1}	IC50 µM	Size	Refs.
Setaria verticillata	MCF7-FLV	18	136	5–20	Current work
Potentilla fulgens	MCF-7	4.91		10–15	Mittal et al. (2015)
Potentilla fulgens	U-87	8.23		10–15	Mittal et al. (2015)
Coleus amboinicus	EAC	30		25.83	Subramanian and Suja (2012)
G. neo-japonicum	MDA-MB-231	6		5–8	John (2013)
Dimocarpus longan	PC-3	10		9–32	Firdhouse and Lalitha (2013), He et al. (2016)
Starch	HCT116		150	142	Satapathy et al. (2013)
Artemisia princeps	A549 cells	18		20	Gurunathan et al. (2015)
Artemisia princeps	L132	50		20	Gurunathan al. (2015)
Origanum vulgare	A549	100		136	Sankar et al. (2013)
Gelidiella sp.	Hep-2	31.25		40–50	Devi et al. (2012)

Table 2 Mortality percentage of Ag-NPs against adult earth worms

Plant derived Ag-NPs	Concentration	% Mortality (1 h)	% Mortality (2 h)	% Mortality (3 h)	*P* value
10 SV	6 μg mL^{-1}	0	0	0	
10 SV	12 μg mL^{-1}	0	25	25	
20 SV	6 μg mL^{-1}	0	25	25	
20 SV	12 μg mL^{-1}	25	25	25	
30 SV	6 μg mL^{-1}	25	50	50	$P < 0.05$
30 SV	12 μg mL^{-1}	50	100	100	
40 SV	6 μg mL^{-1}	50	100	100	
40 SV	12 μg mL^{-1}	50	100	100	
+ve C	0.55 μg mL^{-1} HCl	50	100	100	
−ve C	Phosphate buffer	0	0	0	

Dimocarpus longan show more toxicity than large nanoparticles in Table 1.

The in vitro anthelmintic potential of biosynthesized Ag-NPs was studied in adult earthworms (Lumbricina). This resulted in a statistically significant effect ($P < 0.05$) in Table 2. The 40 SV sample shows 50% mortality of earthworms after 1 h and 100% mortality after 2–3 h. The 30SV samples are more effective at 12 μg mL^{-1} concentration compared to 6 μg mL^{-1}, while both 10 SV and 20 SV samples show 25% mortality of earthworms after 2–3 h. However, this work reveals the cytotoxic effect of NP against the soil organism, Lumbricina, and recommends that proper disposal of the NPs to the environment needs to be planned (Samrot et al. 2017).

Conclusion

In this work, we presented a green method for the biosynthesis of Ag-NPs using seed extract. The physiochemical properties of the resulting silver NPs were characterized as a function of the SV seed extract concentration. Increasing the SV concentrations significantly reduced the NP size. It was found that its toxicity strongly depended on the concentration of SV seed extract. Their toxicity was evaluated using MCF7-FLV cell lines and adult Lumbricina. It was observed that the cytotoxicity of silver nanoparticles increased with increase in the seed extract concentration. The DOX- and DNR-loaded Ag-NPs showed efficient and remarkable loading efficiency (80, 50)% and capacity (40, 25)%, respectively, dependent on electrostatic interaction, surface morphology, H-bonding and ion exchange interaction between ADC and Ag-NPs.

Acknowledgements This work was supported by the Higher Education Commission (HEC), Pakistan, through 5000 indigenous PhD Scholar Program. The microscope analyses were conducted in the ANU Center for Advanced Microscopy (CAM).

Compliance with ethical standards

Conflict of interest The authors confirm that they have no conflict of interest.

References

Amin M, Mostofa M, Hoque M, Sayed M (2009) In vitro anthelmintic efficacy of some indigenous medicinal plants against gastrointestinal nematodes of cattle. JBAU 7(1):57–61. doi:10.3329/jbau.v7i1.4799

Azeez L, Lateef A, Adebisi SA (2017) Silver nanoparticles (AgNPs) biosynthesized using pod extract of Cola nitida enhances antioxidant activity and phytochemical composition of *Amaranthus caudatus*. Linn Appl Nanosci 7:59–66. doi:10.1007/s13204-017-0546-2

Babu MG, Gunasekaran P (2009) Production and structural characterization of crystalline silver nanoparticles from *Bacillus cereus* isolate. Colloids Surf B Biointerfaces 74(1):195. doi:10.1016/j.colsurfb.2009.07.016

Bar H, Bhui DK, Sahoo GP, Sarkar P, Pyne S, Misra A (2009) Green synthesis of silver nanoparticles using seed extract of *Jatropha curcas*. Colloids Surf A Physicochem Eng Asp 348(1):212–216. doi:10.1016/j.colsurfa.2009.07.021

Carlson C, Hussain SM, Schrand AM, Braydich-Stolle LK, Hess KL, Jones RL, Schlager JJ (2008) Unique cellular interaction of silver nanoparticles: size-dependent generation of reactive oxygen species. J Phys Chem B 112(43):13608–13619. doi:10.1021/jp712087m

Daunorubicin (2017) https://commons.wikimedia.org/wiki/File:Daunorubicin.svg. https://commons.wikimedia.org/wiki/File:Daunorubicin_ball-and-stick.png

Devi JS, BhimbA BV, Ratnam K (2012) Invitro anticancer activity of silver nanoparticles synthesized using the extract of Gelidiella sp. Int J Pharm Pharm Sci 4:710–715

Depan D, Shah J, Misra RDK (2011) Controlled release of drug from folate-decorated and grapheme mediated drug delivery system:

synthesis, loading efficiency, and drug release response. Mater Sci Eng C 31:1305–1312. doi:10.1016/j.msec.2011.04.010
Doxorubicin (2017) https://commons.wikimedia.org/wiki/File:Doxorubicin_3D_ball.png. https://commons.wikimedia.org/wiki/File:Doxorubicin2DCSD.svg
Firdhouse MJ, Lalitha P (2013) Biosynthesis of silver nanoparticles using the extract of *Alternanthera sessilis*—antiproliferative effect against prostate cancer cells. Cancer Nanotechnol 4(6):137. doi:10.1007/s12645-013-0045-4
Gurunathan S, Jeong JK, Han JW, Zhang XF, Park JH, Kim JH (2015) Multidimensionaleffects of biologically synthesized silver nanoparticles in *Helicobacter pylori*, *Helicobacter felis*, and human lung (L132) and lung carcinoma A549 cells. Nanoscale Res Lett 10(1):35. doi:10.1186/s11671-015-0747-0
He Y, Du Z, Ma S, Cheng S, Jiang S, Liu Y, Li D, Huang Zhang K, Zheng X (2016) Biosynthesis, antibacterial activity and anti-cancer effects against prostate cancer (PC-3) cells of silver nanoparticles using D*imocarpus Longan Lour*. Nanoscale Res Lett 11(1):1–10. doi:10.1186/s11671-016-1511-9
Holm LG, Plucknett DL, Pancho JV, Herberger JP (1977) The world's worst weeds. University Press, Cambridge
Ismail RA, Almashhadani NJ, Sadik RH (2017) Preparation and properties of polystyrene incorporated with gold and silver nanoparticles for optoelectronic applications. Appl Nanosci 7:109–116. doi:10.1007/s13204-017-0550-6
Jagtap UB, Bapat VA (2013) Green synthesis of silver nanoparticles using *Artocarpus heterophyllus* Lam. seed extract and its antibacterial activity. Ind Crops Prod 46:132–137. doi:10.1155/2013/201057
John P (2013) Green synthesis of silver nanoparticles using Ganoderma neo-japonicum Imazeki: a potential cytotoxic agent against breast cancer cells. Int J Nanomed 8:4399–4413. doi:10.2147/IJN.S51881
Khan AV, Ahmed QU, Mir MR, Shukla I, Khan AA (2011) Antibacterial efficacy of the seed extracts of *Melia azedarach* against some hospital isolated human pathogenic bacterial strains. Asian Pac J Trop Biomed 1(6):452–455. doi:10.1016/S2221-1691(11)60099-3
Kokina I, Gerbreders V, Sledevskis E, Bulanovs A (2013) Penetration of nanoparticles in flax (*Linum usitatissimum* L.) calli and regenerants. J Biotechnol 165(2):127–132. doi:10.1016/j.jbiotec.2013.03.011
Krishna IM, Reddy GB, Veerabhadram G, Madhusudhan A (2016) Eco-friendly green synthesis of silver nanoparticles using *Salmalia malabarica*: synthesis, characterization, antimicrobial, and catalytic activity studies. Appl Nanosci 6(5):681–689. doi:10.1007/s13204-015-0479-6
Lade BD, Patil AS (2017) Silver nano fabrication using leaf disc of *Passiflora foetida* Linn. Appl Nanosci 7:181–192. doi:10.1007/s13204-017-0558-y
Lee KS, El-Sayed MA (2006) Gold and silver nanoparticles in sensing and imaging: sensitivity of plasmon response to size, shape, and metal composition. J Phys Chem B 110(39):19220–19225. doi:10.1021/jp062536y
Lin D, Xing B (2008a) Adsorption of phenolic compounds by carbon nanotubes: role of aromaticity and substitution of hydroxyl groups. Environ Sci Technol 42:7254–7259. doi:10.1021/es801297u
Lin D, Xing B (2008b) Adsorption of phenolic compounds by carbon nanotubes: role of aromaticity and substitution of hydroxyl groups. Environ Sci Technol 42:9005–9013. doi:10.1021/es801777n
Lukman AI, Gong B, Marjo CE, Roessner U, Harris AT (2011) Facile synthesis, stabilization, and anti-bacterial performance of discrete Ag nanoparticles using Medicago sativa seed exudates. J Colloid Interface Sci 353(2):433–444. doi:10.1016/j.jcis.2010.09.088
Magudapathy PP, Gangopadhyay Panigrahi B, Nair K, Dhara S (2001) Electrical transport studies of Ag nanoclusters embedded in glass matrix. Phys B Condens Matter 299(1):142–146. doi:10.1016/S0921-4526(00)00580-9
Mashhadizadeh MH, Diva MA (2012) Drug-carrying amino silane coated magnetic nanoparticles as potential vehicles for delivery of antibiotics. J Nanomed Nanotechol 3:7. doi:10.4172/2157-7439.1000139
Mittal AK, Tripathy D, Choudhary A, Aili PK, Chatterjee A, Singh IP, Banerjee UC (2015) Bio-synthesis of silver nanoparticles using *Potentilla fulgen*s Wall. ex Hook. and its therapeutic evaluation as anticancer and antimicrobial agent. Mater Sci Eng C 53:120–127. doi:10.1016/j.msec.2015.04.038
Nair LS, Laurencin CT (2007) Silver nanoparticles: synthesis and therapeutic applications. JBN 3(4):301–316. doi:10.1166/jbn.2007.041
Navaladian S, Viswanathan B, Viswanath R, Varadarajan T (2007) Thermal decomposition as route for silver nanoparticles. Nanoscale Res Lett 2(1):44. doi:10.1007/s11671-006-9028-2
Priyadharshini RI, Prasannaraj G, Geetha N, Venkatachalam P (2014) Microwave-mediated extracellular synthesis of metallic silver and zinc oxide nanoparticles using macro-algae (*Gracilaria edulis*) extracts and its anticancer activity against human PC3 cell lines. Biotechnol Appl Biochem 174(8):2777–2790. doi:10.1007/s12010-014-1225-3
Ramamurthy C, Padma M, Mareeswaran R, Suyavaran A, Kumar MS, Premkumar K, Thirunavukkarasu C (2013) The extra cellular synthesis of gold and silver nanoparticles and their free radical scavenging and antibacterial properties. Colloids Surf B Biointerfaces 102:808–815. doi:10.1016/j.colsurfb.2012.09.025
Ramar M, Manikandan B, Marimuthu PN, Raman T, Mahalingam A, Subramanian P, Karthick S, Munusamy A (2015) Synthesis of silver nanoparticles using *Solanum trilobatum* fruits extract and its antibacterial, cytotoxic activity against human breast cancer cell line MCF 7. Spectrochim Acta A Mol Biomol Spectrosc 140:223–228. doi:10.1016/j.saa.2014.12.060
Sabeti B, Noordin MI, Mohd S, Hashim R, Dahlan A, Javar HA (2014) Development and characterization of liposomal doxorubicin hydrochloride with palm oil. BioMed Res Int Hindawi Publ Corp. doi:10.1155/2014/765426
Samrot AV, Justin C, Padmanaban S, Burman U (2017) A study on the effect of chemically synthesized magnetite nanoparticles on earthworm: *Eudrilus eugeniae*. Appl Nanosci 7:17–23. doi:10.1007/s13204-016-0542-y
Sankar R, Karthik A, Prabu A, Karthik S, Shivashangari KS, Ravikumar V (2013) *Origanum vulgare* mediated biosynthesis of silver nanoparticles for its antibacterial and anticancer activity. Colloids Surf B Biointerfaces 108:80–84. doi:10.1016/j.colsurfb.2013.02.033
Satapathy SR, Mohapatra P, Preet R, Das D, Sarkar B, Choudhuri T, Wyatt MD, Kundu CN (2013) Silver-based nanoparticles induce apoptosis in human colon cancer cells mediated through p53. Nanomedicine 8(8):1307–1322. doi:10.2217/nnm.12.176
Sharma G, Jeevanandam P (2013) A facile synthesis of multifunctional iron oxide@ Ag core–shell nanoparticles and their catalytic applications. Eur J Inorg Chem 36:6126–6136. doi:10.1002/ejic.201301193
Sims RW, Gerard BM (1985) Earthworms: keys and notes for the identification and study of the species. Brill Archive, Leiden
Smetana AB, Klabunde KJ, Sorensen CM (2005) Synthesis of spherical silver nanoparticles by digestive ripening, stabilization with various agents, and their 3-D and 2-D superlattice formation. J. Colloid. Interface Sci 284(2):521–526. doi:10.1016/j.jcis.2004.10.038

Söderstjerna E, Bauer P, Cedervall T, Abdshill H, Johansson F, Johansson UE (2014) Silver and gold nanoparticles exposure to in vitro cultured retina–studies on nanoparticle internalization, apoptosis, oxidative stress, glial-and microglial activity. PLoS One 9(8):e105359. doi:10.1371/journal.pone.0105359

Subramanian V, Suja S (2012) Green synthesis of silver nanoparticles using *Coleus amboinicus* lour, antioxidant activity and in vitro cytotoxicity against Ehrlich's ascite carcinoma. J Pharm Res 5(2):3–1272

Teo JY, Chin W, Ke X, Gao S, Liu S, Cheng W, Hedrick JL, Yang YY (2017) pH and redox dual-responsive biodegradable polymeric micelles with high drug loading for effective anticancer drug delivery. Nanomedicine 13:431. doi:10.1016/j.nano.2016.09.016

Tolaymat TM, El Badawy AM, Genaidy A, Scheckel KG, Luxton TP, Suidan M (2010) An evidence-based environmental perspective of manufactured silver nanoparticle in syntheses and applications: a systematic review and critical appraisal of peer-reviewed scientific papers. Sci Total Environ 408((5):999–1006. doi:10.1016/j.scitotenv.2009.11.003

Upendra KS, Amita V, Sunil KP, Himanshu P, Avinash CP (2015) In vitro, in vivo and pharmacokinetic assessment of amikacin sulphate laden polymeric nanoparticles meant for controlled ocular drug delivery. Appl Nanosci 5:143–155. doi:10.1007/s13204-014-0300-y

Velmurugan P, Shim J, Kamala-Kannan S, Lee KJ, Oh BT, Balachandar V (2011) Crystallization of silver through reduction process using *Elaeis guineensis* biosolid extract. Biotechnol Prog 27(1):273–279. doi:10.1002/btpr.511

Yu D-G (2007) Formation of colloidal silver nanoparticles stabilized by Na+–poly (γ-glutamic acid)–silver nitrate complex via chemical reduction process. Colloids Surf B 59(2):171–178

Zamiri R, Zakaria A, Abbastabar H, Darroudi M, Husin MS, Mahdi MA (2011) Laser-fabricated castor oil-capped silver nanoparticles. Int J Nanomed 6:565–568. doi:10.2147/IJN.S16384

Zhang J, Gu M, Zheng T, Zhu J (2009) Synthesis of Gelatin-stabilized gold nanoparticles and assembly of carboxylic single-walled carbon nanotubes/Au composites for cytosensing and drug uptake. Anal Chem 81:6641–6664. doi:10.1021/ac900628y

Zhang J, Cheng F, Lib J, Zhub J, Lu Y (2016) Fluorescent nanoprobes for sensing and imaging of metal ions: recent advances and future perspectives. Nanotoday 11:309–329. doi:10.1016/j.nantod.2016.05.010

Zhang J, Cheng F, Zheng T, Zhu J (2017) Versatile aptasensor for electrochemical quantification of cell surface glycan and naked-eye tracking glycolytic inhibition in living cells. Biosens Bioelectron 89:937–945. doi:10.1016/j.bios.2016.09.087

Publisher's Note